Journal of Materials Chemistry B

Accepted Manuscript

ROYAL SOCIETY OF CHEMISTRY

www.rsc.org/materialsB

Biofunctionalized quantum dots-nickel oxide nanorods based smart platform for lipid detection

Md. Azahar Ali[1,2], Saurabh Srivastava[1,4], Ved V. Agrawal[1], Magnus Willander[3], Renu John[2], Bansi D. Malhotra[4]*

[1]*Department of Science and Technology Centre on Biomolecular Electronics, Biomedical Instrumentation Section, CSIR-National Physical Laboratory, Dr. K. S. Krishnan Marg, New Delhi 110012, India*
[2]*Indian Institute of Technology Hyderabad, Ordnance Factory Estate, Yeddumailaram, Hyderabad, Andhra Pradesh 502205, India*
[3]*Department of Science & Technology, Division of Physics & Electronics Linkoping University, SE60174,Sweden*
[4]*Department of Biotechnology, Delhi Technological University, Shahbad Daulatpur, Main Bawana Road, Delhi110042, India*

A reagent-free, low-cost and sensitive immunosensor has been fabricated using anti-apolipoprotein B (AAB) conjugated L-cysteine *in situ* capped cadmium sulfide quantum dots (CysCdS QDs) bound to nickel oxide nanorods (nNiO) for detection of low density lipoprotein (LDL) molecules in human serum samples. The structural and morphological properties of AAB conjugated CysCdS QDs and nNiO have been determined using electron microscopy, X-ray diffraction, Fourier transform infrared spectroscopy and UV-visible techniques. In this immunosensor, the synthesized NiO nanorods act as mediators that allow the direct electron transfer due to their channeling effect resulting in a mediator-free biosensor. This mediator-free CysCdS-NiO based immunosensor shows improved characteristics such as good sensitivity of 32.08 $\mu A/mgdl^{-1}/cm^2$ compared to that based on nNiO (1.42 $\mu A/mgdl^{-1}/cm^2$) alone for detection of lipid (LDL) molecules in a wide concentration range, 5-120 mg/dl (0.015-0.36 µM). The kinetic analyses yields value of the association constant (K_a) as 3.24 kM^{-1} s^{-1} indicating that the antibody conjugated CysCdS-NiO platform has a strong affinity towards lipid molecules. The excellent electron transport properties of the CysCdS-NiO nanocomposite in this immunosensor reveal that it provides an efficient platform for routine quantification of LDL molecules in real samples.

Keywords: Mediator-Free, L-Cysteine, CdS quantum dots, NiO nanorods, Lipid molecules, Anti-apolipoprotein B, Immunosensor

Corresponding Author: Bansi D. Malhotra, **E-mail**: bansi.malhotra@gmail.com

1. Introduction

The semiconductor quantum dots (QDs) have recently aroused much interest for development of miniaturized nano-bioelectronic devices due to their tunable size.[1-2] The size of a QD ranges from one to ten nanometers and the dimensions are usually smaller than the de Broglie wavelength.[3-4] The QDs have been predicted to be interesting nanomaterials for the development of electro-optical devices including biosensors due to their high surface reactivity, wide absorption and the narrow emission band spectra of QDs with excellent photostability, dispersibility and quantum yield. The applications of QDs are being increasingly explored for *in vitro* diagnostics and *in vivo* imaging of tumors, immunohistochemistry, DNA hybridization, cell imaging, bioluminescence, resonance energy transfer and biosensors.[5-8] However, toxicity of the cadmium based QDs is currently an increased concern since it yields limited shelf-life of a biosensor.[9] Different strategies have been attempted to explore the preparation of multiplexed QDs based immunoprobes *via* electrostatic adsorption of antibodies on the outermost surface of QDs.[1] Xing *et al.* have demonstrated bioconjugation of multicolor QDs with antibodies for quantitative and multiplexed immunohistochemistry.[8]

The bioconjugated quantum dots can be utilized for the fabrication of immunosensors. However, conjugation of the biomolecules with QDs is currently a major concern. In addition, QDs can be made water miscible via coating with ampliphilic polymers or by ligand exchange that can be linked to small proteins, peptides, nucleic acids, carbohydrates, antibodies and other biomolecules.[10] The bioconjugation of QDs with cancer-specific folic acid and herceptin (antibodies) can be used for selective imaging of the human cancer such as that of breast, prostate, pancreatic cancer etc.[11] In particular, cadmium sulfide (CdS) QDs were recently used for development of

electrochemical biosensors due to their remarkable electrochemical properties.[12-14] Qiant *et al.* fabricated an electrochemical glucose biosensor based on nanostructured CdS that served as a mediator for electron transfer *via* channeling effect.[15] Ali *et al.* recently reported CdS based electrochemical and optical platforms to investigate the antigen-antibody interactions.[16] QDs can provide an excellent redox activity due to higher charge detaching efficiency and synergetic effect that may lead to improved performance of a biosensor.[16]

Nanostructured nickel oxide (nNiO) offers attractive properties such as large surface-to-volume ratio, high electro-catalytic property and does not degrade on its exposure to proteins.[17] The electronic conduction of nanorods-like geometry of NiO occurs due to many processes including bulk conduction, tunneling mechanism, the enhanced surface scattering of electrons and high density of electronic states.[18] The nNiO provides high isoelectric point (IEP~10.8) that can be utilized to immobilize the antibodies (IEP~4.5) *via* electrostatic interactions or attachment with a nanomaterial (e.g CdS) that has a negative electrokinetic surface potential. The majority of metal oxide nanomaterials including TiO_2, ZrO_2, ZnO exhibit semiconducting nature that is advantageous for the biosensor development, due to enhanced electrochemical signal.[19-20] The presence of variable oxidation state in the nNiO may provide easy mobility of electrons resulting in a mediator-free or third generation electrochemical biosensor.[21] Ali *et al.* recently reported a microfluidic based biochip using NiO nanorods patterned microelectrode for direct immobilization of cholesterol oxidase.[17] Attempts were made to utilize the CdS-metal oxide nanohybrid due to its interesting photocatalytic activity.[22-23] Wang *et al.* reported CdS QDs-sensitized TiO_2 nanorods array based on transparent conductive glass photoelectrode and investigated their photoelectrochemical properties.[24]

The bioconjugated CdS QDs and nanostructured metal oxide composite platform may result in the development of a third generation mediator-free biosensor.

The low and high level of LDL concentration in human blood can cause coronary heart and vascular diseases. The cholesterol in human serum is a clinically important parameter for the point-of-care diagnostics.[25-27] Matharu *et al.* used apolipoprotein-B functionalized 4-aminothiophenol for LDL detection using quartz crystal microbalance and surface plasmon resonance techniques.[28] Jie *et al.* developed an electroluminescence immunosensor based on apolipoprotein B functionalized CdS nanocrystal for LDL detection.[29] The silver chloride@polyaniline core-shell nanocomposite coated with gold nanoparticles based platform was explored for detection of LDL molecules.[30] A high density lipoprotein biosensor was developed by Chammem *et al*.[31] To achieve high sensitivity, these sensing platforms require presence of a $[Fe(CN)_6]^{3-/4-}$ redox couple for transfer of electrons in the medium. A gold sensing layer on screen printed electrode containing immobilized monoclonal antibodies of oxidized LDL were proposed for detection of LDL molecules in the range, 0.5 -18.0 mg mL^{-1}.[32] The carbon nanotubes coated with chitosan reveal a detection limit of 12.5 mg/dl for LDL molecules.[33] For the mediator based biosensors, the sensitivity, limit of detection, and selectivity of these immunosensors are presently a major concern.

We demonstrate the fabrication of a mediator-free immunosensor using NiO nanorods *via* electrophoretic deposition. The antiapolipoprotein-B (AAB) conjugated L-cysteine (Cys) capped CdS QDs were immobilized on the surface of NiO nanorods by physical adsorption. Capping of CdS QDs by L-cysteine results in decreased agglomeration and provides negative surface potential and may directly interact electrostatically with the positively charged NiO nanorods. The fabricated CdS-NiO based immunoelectrode has

been utilized for the first time for detection of LDL molecules by amperometric technique. Bovine serum albumin (BSA) treatment blocks the non-specific sites of immunoelectrode (BSA-AAB/CysCdS-NiO). We have also carried out studies relating to analytical performance of biosensors based on nNiO and CysCdS-NiO nanorods smart composite for quantification of LDL molecules in the real human serum samples.

2. Materials and methods

2.1 Chemicals and reagents

All chemicals were purchased from Sigma Aldrich, USA. Nickel nitride [$Ni(NO_3)_2$], cadmium chloride ($CdCl_2$), sodium sulfide (Na_2S) and L-cysteine was from Fisher Scientific, USA. Anti-apolipoprotein B-100 (AAB; MW: 515 kDa), LDL (MW: 3500 kDa), BSA, N-hydroxysuccinimide (NHS), N-ethyl-N0-(3-dimethylaminopropyl carbodiimide) (EDC) were procured from Sigma–Aldrich, USA. Distilled water was from Millipore water purification system. 5 mg of lyophilized powder (LDL) was dissolved in 1 ml of de-ionized water that contains 150 mM NaCl of pH 7.4 and 0.01% ethylenediaminetetraacetic acid (EDTA). The BSA (2 mg/ml) solution was obtained in 50 mM phosphate buffered saline (PBS) pH 7.4 containing 150 mM NaCl. 1 mg/ml solution of AAB was prepared in 50 mM PBS of pH 7.4 containing 150 mM NaCl.

2.2 Synthesis of *in situ* L-Cysteine Capped CdS QDs

For synthesis of L-cysteine *in situ* capped CdS QDs, we first prepared 50 ml of $CdCl_2$ (1.7 mg/ml) solution using deionized water under continuously stirred condition. 100 µl of L-cysteine solution (0.02 mol/l) was added drop wise to $CdCl_2$ solution with continuous stirring under nitrogen atmosphere.[34] After 50 min, Na_2S solution (1.5 mg/ml) was added drop wise and continuously stirred until the solution became light yellow in color resulting in L-cysteine capped CdS precipitation with pH 2.5. The NaOH solution

was added to adjust pH 8.0. This yellow L-cysteine capped CdS precipitate was again filtered and washed several times using de-ionized water and well dispersed in 50 µl of ethylene glycol solution *via* 2h sonication and stored at 4°C when not in use.

2.3 Immunosensor fabrication

The NiO nanorods powder was synthesized using co-precipitation method.[17] The NiO nano-powder was well-dispersed in acetonitrile (0.6 mg/ml) *via* sonication (5 h). The colloidal solution of NiO nanorods was used for electrophoretic deposition (EPD) *via* a two electrodes glass cell comprising of platinum foil as the counter electrode (anode) and a hydrolized-ITO coated glass plate as the working electrode (cathode). On application of field (potential: 67 V for 2 min), the positively charged NiO nanoparticles were deposited onto ITO substrate (size: 0.25 cm^2) after which it was removed from the cell and washed with de-ionized water and dried. In order to obtain surface charges on NiO nanorods, 10^{-5}–10^{-4} mol of Mg $(NO_3)_2.6H_2O$ was added into the suspension as an electrolyte during EPD. 20 µl of well-dispersed colloidal solution of the *in situ* synthesized L-cysteine capped CdS QDs was spread on the NiO film surface *via* physical adsorption. The -COOH functional groups were activated using EDC-NHS chemistry in which EDC (0.2M) worked as a coupling agent and NHS (0.05M) acted as an activator. The L-cysteine capped CdS QDs onto nNiO film was stored at 4 °C for 4 h resulting in electrostatic interaction (Schematic 1) between nNiO film (positively charged) and CysCdS QDs (negatively charged). The AAB solution (10 µl) was spread onto CysCdS-NiO/ITO surface followed by EDC-NHS chemistry and kept for 4 h in a humid chamber. The –COOH terminal of AAB and $-NH_2$ terminal of CysCdS-NiO covalently interact with each other resulting in formation of strong covalent amide bond. For control measurements, the CysCdS quantum dots were drop cast onto the surface of ITO

electrode without nNiO and covalently attached with the antibodies (AAB). Lastly, the BSA solution was used for blocking non-specific sites of the antibody functionalized surface. The BSA-AAB/CdS and BSA-AAB/CdS-NiO based immunosensors were kept at 4 °C when not in use.

2.4 Instrumentation

The CysCdS-NiO and the AAB- functionalized CysCdS-NiO were characterized using X-ray diffraction (XRD, Cu Kα radiation, Rigaku), and transmission electron microscopy (TEM, JEOL JEM-2000 EX). The optical properties were carried out using UV-visible (Perkin Elmer, Model Lamda 950 and Fourier-transform infrared spectroscopy (FT-IR; Perkin-Elmer, Model 2000). Zeta potential measurements were conducted using Zetasizer (Malvern, Model ZEN 3690). The electrochemical investigations of the prepared immunoelectrode with and without nNiO were conducted using an Autolab Potentiostat/Galvanostat (Model AUT-84275) using a three electrode electrochemical cell system consisting of a working electrode (ITO), Ag/AgCl as a reference electrode and platinum foil as a counter electrode.

3 Results and discussion

3.1 Structural studies

The results of XRD studies [Figure 1(i)] reveal the purity and crystallinity of the synthesized NiO film (spectra a) with the face-centred cubic (*a*) 4.1 Å and space group $Fm\bar{3}m$ (225), [JCPDS Card No. 89-5881]. The observed reflection peaks found at (200), (220), (311), (400) and (222) planes are attributed to cubic structure of the NiO nanorods. It appears that the NiO film is largely dominated by (220) facets indicating preferred crystallization along the plane (220). The d_{111} value of NiO film is found to be 0.29 nm

for the (220) plane. The peaks seen at 31.5°, 32.9°, 45.3°, 50.9° and 60.5° correspond to the planes (12$\bar{1}$), (300), (401), (124) and (143) [JCPDS Card No. 89-4599] arising due to indium tin oxide coating on the glass substrate. The XRD pattern of the CysCdS-NiO film shows additional diffraction peaks at 43.2°, 54.2°, 67.2° and 69.1° that may be associated with (110), (004), (203) and (201) [JCPDS (6–314)] planes, respectively, due to incorporation of CysCdS in NiO (spectra b). Two crystallographic forms of CysCdS QDs are namely hexagonal (Wurtzite) and cubic (Zinc blend). The diffraction pattern of CdS-NiO film shows mixed hexagonal and cubic phase. The other reflection planes are due to ITO coating on the glass substrate.

In the Fourier transform-infrared **(**FT-IR) spectra, the peak found at 500 cm^{-1} in the finger print region (spectra a) corresponds to vibration bending of Ni-O [Figure 1(ii)]. The small peaks found at 1238 and 1382 cm^{-1} arise due to the physical adsorption of CO_2 on nNiO film surface. In the spectra (b), the intense peak at 532 cm^{-1} in the finger print region is due to incorporation of CysCdS nanocrystals onto the nNiO film. The peaks seen at 1152, 1644 and 1787 cm^{-1} corresponding to stretching vibrations of C-O, C=C and C=O bonds, respectively, arise due to presence of the carboxylic acid in CysCdS QDs. The small peak found at 2600 cm^{-1} corresponds to the S-H stretching due to CysCdS QDs. The peaks observed at 1521 and 3371 cm^{-1} are attributed to amide N-H (I and II) bands indicating antibody (AAB) and BSA functionalization of the CdS-NiO (spectra c). The peak seen at 1079 cm^{-1} is assigned to C-N stretching band of amine that may be due to presence of covalent interaction between carboxylic group (-COOH) in CysCdS QDs and amide (NH_2) in AAB and BSA. These results reveal that CdS QDs conjugated with the antibodies are immobilized on the surface of NiO film.

In the UV-visible spectra of CysCdS quantum dots [Figure 1(iii)], the magnitude of absorption increases from 500 to 245nm (spectra a). The radius (R) of CysCdS quantum dot can be evaluated using effective mass approximation model [Eq. 1].[16]

$$\Delta E = (\hbar^2\pi^2/2R^2)\left(\frac{1}{m_e}+\frac{1}{m_h}\right) - \frac{1.8e^2}{\varepsilon R} \quad (1)$$

where ΔE is the increase in band gap energy, ε =5.7 is the relative dielectric constant, and m_e =0.19 m_0 and m_h =0.8m_0 are the effective masses of electrons and holes, respectively. It has been found that radius of CysCdS QDs is less than 6 nm. The strong absorption peak seen at 330 nm (spectra b) corresponds to 3d electronic transition of Ni^{2+} in the cubic structure of NiO. The blue shift of the absorption edge compared to that of the bulk NiO reveals the quantum size effect resulting due to growth of the nanorods. The direct band gap (E_g) of these synthesized NiO nanorods is found to be as 3.29 eV using Tauc equation. The absorption intensity of CysCdS-NiO increases from 600 nm to lower wavelength, revealing the formation of CysCdS-NiO nanocomposite (spectra c).

Zeta potential measurements were conducted to confirm the surface electrokinetic potential of the synthesized CdS QDs (a), Cys-CdS QDs in ethylene glycol (b) and NiO nanorods in acetonitrile (c) [Supplementary data, Figure S1]. The zeta potential of CdS QDs is found to be as -0.05 mV. After capping with L-cysteine, the CdS QDs show slightly negative zeta potential as -1.0 mV due to attachment of L-cysteine containing –COOH and -NH_2 group with CdS QDs. The zeta potential is obtained as positive (+10.0 mV) for NiO nanorods dispersed in solution (c). These results indicate that L-cysteine capped CdS QDs can be attached directly with NiO nanorods due to opposite surface potential resulting in electrostatic interaction between them.

3.2 Morphological studies

Figure 2 shows TEM image of the synthesized NiO nanorods ultrasonically prepared by dispersing it in methanol and placing it on the surface of copper grid coated amorphous carbon film *via* drop casting method followed by drying it in air. Image (a) shows an overview of the NiO nanorods bundle. The majority of NiO nanorods exhibit nearly straight line. The individual NiO nanorod with aspect ratio of about ~8 is shown in the inset of image (a). The morphology and structure of an individual nanorod of size (length=40 nm; diameter=5nm) were investigated under high-magnification. The lattice fringes illustrate that the nanorods are highly crystalline and the spacing between the two adjacent lattice fringes is found to be as 0.25 nm for the (220) plane [Figure 2(a), inset] resulting in anisotropic growth of the nanorods along the (220) direction. The image (b) indicates presence of non-uniformly distributed and spherically shaped CysCdS QDs arising due to the capping agent (L-cysteine). The average size of the CysCdS QDs varies from 5 to 7nm. The high magnification image of CysCdS QDs is shown in Figure 2(b, inset). Figure 2(c) shows that CysCdS nanoparticles are attached with NiO nanorods. It appears that CysCdS QDs bind with edges of the NiO nanorods *via* electrostatic interactions arising due to positive surface potential of NiO and negatively charged CysCdS QDs. The high magnification image [Figure 2(d)] of CysCdS-NiO shows the existence of the lattice fringes. The selected area electron diffraction (SAED) pattern consists of various diffraction rings with different radii [Figure 2(e)]). The consecutive rings appearing in the SAED pattern correspond to (111), (200), (220), (311), and (222) planes for NiO and (102), (110), (101), (200) and (104) for CysCdS. The SAED pattern of the CysCdS-NiO is in agreement with the results of XRD studies.

The results of energy-dispersive X-ray (EDX) studies confirm the presence of Ni (39.0 %) and O (42.0 %) elements in nNiO film [Fig. S2 (a and inset)]. After CysCdS incorporation into the NiO film, it appears that CdS QDs are of spherical shape and are distributed onto NiO surface [Figure S2 (b, inset)]. Further, EDX pattern of CysCdS-NiO film confirms the presence of Cd and S elements on NiO film [Figure S2 (c)]. The EDX spectra of the AAB immobilized CysCdS-NiO film shows additional elements such as N, Na, Ca and Cl arising due to antibody immobilization on the surface of CysCdS QDs. The presence of additional peak pertaining to nitrogen confirms the antibody immobilization of CysCdS-NiO surface. Table S1 shows atomic ratio (%) of the elements for the various fabricated films (Supplementary data).

3.3 Direct electrochemistry

The cyclic voltammetry (CV) studies of the fabricated electrodes were conducted in PBS, 50 mM (pH 7.0, 0.9% NaCl) in the potential range from -0.5V to +1.0V [Figure 3(i)]. The electrode exhibits well-defined oxidation and reduction peaks without using any mediator. The magnitude of current peak for the bare ITO electrode is found to be as 0.356 µA [Figure S3, Supplementary data] at oxidation potential of +0.44V. The curve (a) shows variation of the anodic and cathodic current peaks pertaining to nNiO film deposited at the ITO electrode [Figure 3(i)]. The magnitude of peak current increases to 33.7µA and the oxidation potential shifts to lower value (+0.2V). The NiO nanorods act as a mediator for direct transfer of electrons toward electrode due to presence of conducting electronic paths resulting in decreased electron tunneling distance to facilitate diffusion of electrons leading to enhanced current. Salimi *et al.* have demonstrated direct electron transfer and electrocatalytic activity of NiO nanoparticles in the presence of glucose oxidase.[21] The CysCdS-NiO electrode exhibits higher peak (anodic/cathodic)

current compared to that of the NiO/ITO electrode (curve b). This can be attributed to the presence of CdS that contains S^{-2} ions that provide excellent electrocatalytic redox behavior resulting in enhanced current. However, in case of curve (c), the peak current decreases due to insulating properties of antibodies that hinder electron transfer towards the electrode. After BSA immobilization (curve d), the peak current further decreases due to insulating nature of BSA molecules that block non-binding sites of the immunoelectrode.

The CV studies have been conducted on the BSA-AAB/CdS-NiO immunoelectrode as a function of scan rate in the range of 20-100mV/s [Figure 3(ii)]. Anodic and cathodic peak current vary proportionally with square root of scan rate [Eq. (2-3)] and peak potential shifts towards higher value indicating diffusion controlled process. The redox peak potential shifts (anodic peak potential towards positive potential side and cathodic peak potential towards negative potential side) as the scan rate increases from 20 to 100 mV/s [Fig. S4, Supplementary data]. The value of ΔE_p increases as the sweep rate increases, revealing that electron transfer kinetics has a quasi-reversible behavior. The proportional increase in the anodic and cathodic peak potential as a function of square root of scan rate indicates that the electrochemical reaction follows diffusion controlled process. The values of the slope, intercept and correlation coefficient are given by Eq. (2) and (3).

$$i_a = -5.56\ \mu A + 3.39\ \mu A/(\ mV/s)^{1/2} \times\ [\text{Scan rate } (mV/s)^{1/2}];\quad r^2: 0.996 \qquad (2)$$

$$i_c = 2.80\ \mu A - 5.29\ \mu A/(\ mV/s)^{1/2} \times\ [\text{Scan rate } (mV/s)^{1/2}];\quad r^2: 0.992 \qquad (3)$$

where i_a and i_c are the anodic and cathodic peak current, respectively. The charge associated with the adsorption or desorption of an adsorbate gives an indication of the number of surface catalytic atoms present in the matrix. The electrical charge (Q) is

defined as $Q = \int I\, dt$, where, I is the integral of cell current with respect to time (t). The concentration of BSA-AAB associated with the CysCdS-NiO surface can be determined using the relation, $\Gamma = Q/nFA$, where A is electrode area, Γ is the number of mol/cm^2, Q is the charge obtained by integrating the anodic peak, n is the number of electrons involved in the reaction and F is Faraday constant. The surface concentration of the BSA-AAB/CdS-NiO and CysCdS-NiO electrode is obtained as 2.85×10^{-8} mol/cm^2 and 7.96×10^{-8} mol/cm^2, respectively, indicating that the BSA-AAB strongly interacts with the CdS-NiO surface. The surface concentration of the AAB/CdS-NiO immunoelectrode is estimated to be as 5.6×10^{-8} mol/cm^2. The modified Kochi expression for heterogeneous electron transfer rate constant (k^0) is given by Eq. (4)

$$k^0 = (2.18)\left(\frac{\alpha DnF\upsilon}{RT}\right)^{1/2} exp\left[\frac{-\alpha^2 nF}{RT}\left(E_{pa} - E_{pc}\right)\right] \quad (4)$$

where, E_{pa}, E_{pc} are the anodic and cathodic peak potential, D is diffusion coefficient, υ is scan rate and α is transfer co-efficient (0.5). The k^0 for BSA-AAB/CdS-NiO is obtained as 1.43×10^{-7} cm s^{-1} which is lower than that of the CysCdS-NiO electrode (2.2×10^{-7} cm/s) indicating slow diffusion of electrons kinetics at electrode surface.

3.4 Impedance analysis

The EIS studies provide an effective method to obtain Faradic impedance between electrode and electrolyte interface. Figure 3(iii) shows the Nyquist plots obtained for different electrodes in the frequency range, 0.01–10^5 Hz (0.2 V potential). The semicircle diameter of EIS spectra gives the value of charge transfer resistance (R_{CT}) in the higher frequency range that can be used to obtain information on electron transfer kinetics of the redox probe at the electrode interface. In the Nyquist plot, a linear straight line at 45° to the real axis (Z') at lower frequencies indicates diffusion limited transfer process. The R_{CT} value of an electrode depends on dielectric characteristics of the electrode/electrolyte

interface. The R_{CT} value of the NiO/ITO electrode (curve a) is found to be as 80 Ω. After CySCdS incorporation onto NiO/ITO electrode, the Nyquist plot becomes nearly straight line (curve b) revealing that electron transfer is mainly dominated by diffusion due to the CySCdS-NiO hybrid. After immobilization of the AAB, the R_{CT} value decreases again to 148 Ω (curve c) due to coating of antibodies on the transducer surface that obstructs electron transfer towards the electrode. Again, BSA immobilized immunoelectrode (curve d) results in increased charge transfer resistance due to insulating nature of BSA that blocks non-specific binding sites of antibodies. The surface coverage of these electrodes has been calculated using the relation[25] , $\theta = 1-R_{ct}(\text{electrode})/R_{ct}(\text{bioelectrode})$. About 80% of the surface of CdS-NiO appears to be covered after immobilization of BSA-AAB proteins.

4. Sensor response studies

The cyclic voltammetry (CV) response of the immunosensor with and without nNiO was measured on successive addition of lipid (LDL) concentration [5-120 mg/dl or 0.015-0.36 μM] at a scan rate 30 mV/s [Figure 4 (i and iii)] with incubation time of about five minutes at 25 ºC. Schematic 1 shows the working principle of the fabricated immunosensor. The peak current obtained for both BSA-AAB/CysCdS (ii) and BSA-AAB/CdS-NiO (iv) immunoelectrode increases on addition of LDL concentration (Fig. 4). This is due to increased interaction between LDL molecules and AAB (antibodies) that may promote spatial orientation due to introduction of the easy conducting paths for electron transfer to the electrode surface. Interestingly, Okuno *et al*. observed increased peak current during CV measurement as a function of antigen (prostate-specific) concentration.[35] And it appears that formation of the antigen-antibody complex[36-37] between LDL and AAB on transducer surface provides a favorable orientation that

enables facile charge transfer to the electrode surface resulting in enhanced current. Figure 4(ii and iv) shows calibration plots of fabricated immunosensors that represent the anodic peak currents of the immunoelectrodes versus LDL concentration [5-120 mg/dl]. Figure 4(v) shows a comparison plot for magnitude of current with LDL concentration for this immunosensor with and without nNiO. To provide further evidence, we have conducted the EIS measurements for this fabricated immunosensor as a function of LDL concentration. Figure S5 (a and b, Supplementary data) shows the EIS spectra and response plot in between charge transfer resistance (R_{ct}) and LDL concentration. Compared to CV response studies, we observed an opposite phenomena for the impedance studies. For impedance studies, the charge transfer resistance (R_{ct}) is found to decrease with increasing LDL concentration. This may be due to the increased current generated from the antigen-antibody interactions as described in CV response studies.

This immunosensor with and without incorporation of nNiO shows high sensitivity of 32.08 μA/mgdl^{-1}/cm^2 and 1.42 μA/mgdl^{-1}/cm^2, respectively, the detection range as 5–120 mgdl^{-1}. The CysCdS-NiO hybrid matrix exhibits excellent electrochemical properties resulting in higher sensitivity compared to that based on CysCdS matrix alone. The immunosensor with and without incorporation of nNiO can be used to detect low LDL concentration of 0.05 mg/dl (0.15 mM) and 1.6 mg/dl (4.8 mM), respectively. The improved performance of the CysCdS-NiO based smart immunosensor is due to inherent electrochemical properties of NiO nanorods as compared to that of the CysCdS matrix alone. The limit of quantification (LOQ=10×standard deviation/slope) for the CysCdS-NiO based immunosensor is calculated to be as 0.19 mg/dl. Table 1 shows the sensing parameters of the fabricated immunosensing device alongwith those reported in literature. The value of the association constant (k_a) and the disassociation constant (k_d)

for CysCdS QDs-NiO based immunosensor have been determined as 3.24 kM^{-1} s^{-1} and 0.275 s^{-1}, respectively, indicating high affinity of antibody (AAB) towards LDL molecules. The equilibrium constant (K_a) for association (k_a/k_d) is estimated to be as 11.7 kM^{-1}. Figure 4(vi) shows CV response of the BSA-AAB/CdS-NiO immunoelectrode for real serum samples containing LDL and the histogram plot obtained for the current response for both real and synthetic samples is shown in the inset. The real serum samples containing various concentration of LDL molecules were investigated by the prepared immunosensor (Table 2). The low relative standard deviation (less than 5%) of immunosensor response for real serum and standard solutions indicates excellent performance. These studies indicate that this interesting CdS-NiO based immunosensor can be used to detect LDL concentration in human serum samples in the physiological range of human blood (<129 mg/dL).

The reproducibility of the immunosensor (BSA-AAB/CdS-NiO) was investigated using different working electrodes under similar conditions with LDL concentration (60 mg/dl) [Figure S6, (i)]. The immunosensor shows good reproducibility for different electrodes (six) with constant sensor surface area as evidenced by relative standard deviation (RSD) of 0.32% (mean value = 23.06 µA). The low RSD value of this fabricated immunosensor indicates good precision. The stability of the immunosensor was determined by measuring the current value at regular intervals of time for 90 days [Figure S6, (ii)]. The current response of the immunoelectrode was found to decrease (5.3%) in about 40 days. However, after 90 days the current value decreased to about 25% from the initial value. The CdS-NiO and CysCdS based immunoelectrodes were tested with LDL concentration (60 mg/dL) alongwith different inteferents such as free cholesterol, total cholesterol, and triglyceride (Figure S7). The CdS-NiO and CysCdS

QDs based immunoelectrodes did not show any significant variation in current in the presence of these interferents as evident by low RSD of 6% and 5.9 %, respectively.

Table 1. Sensing performance of BSA-AAB/CysCdS-NiO immunoelectrode alongwith those reported in literature.

Electrodes	**Detection technique**	**Detection range**	**Sensitivity**	**Association constant**	**Ref.**
B-HEP/AVI/ATP/Au	SPR	20-100 mg/dl	0.014 m°/ $mgdl^{-1}$		[37]
HEP/ATP/Au	SPR	10-120 mg/dl	21.0 m°/$mgdl^{-1}$	96.7 M^{-1} s^{-1}	[28]
AAB/ATP/Au	QCM	10-84 mg/dl	0.012 Hz/$mgdl^{-1}$	4.437 $kM^{-1}s^{-1}$	[36]
AAB/AuNPs-AgCl@PANI	EIS	3.4 -134 ng/dl	……	……	[30]
BSA-AAB/CdS-NiO	CV	5-120 mg/dl	8.02 µA/$mgdl^{-1}$	3.24 kM^{-1} s^{-1}	Present work

Table 2 The current response of LDL real sample in serum and standard solution of LDL for BSA-AAB/CdS-NiO immunoelectrode.

LDL concentration (mg/dl)	**Current with standard solution (µA)**	**Current with serum sample (µA)**	**% RSD**
5	14.58	14.98	1.91
15	18.61	18.72	0.42
30	20.94	21.50	1.87
60	23.13	23.95	2.46
90	24.92	26.72	4.93
120	25.71	25.94	0.63

5. Conclusions

A label-free immunosensor has been fabricated using AAB conjugated CdS QDs and NiO nanorods composite platform for detection of lipid profile in human serum samples. The NiO nanorods act as a mediator indicating direct electron transfer toward the electrode due to channeling effect. Besides this, the conjugated CdS nanocrystal-based NiO hybrid matrix exhibits excellent electrochemical activity compared to that based on CdS QDs

alone resulting in a mediator-free third generation biosensor (immunosensor). The use of capping agent (L-cysteine) results in decreased agglomeration of CdS QDs that provide negative surface potential resulting in high affinity to interact electrostatically with the positively charged NiO nanorods. The covalent coupling of CdS QDs allows it to be stabilized by minimizing the surface energy via "capping" and can be bound to the desired target (antibodies). The fabricated immunosensor has been found to be highly selective, sensitive and exhibits detection range of 5-120 mg/dl of LDL concentration that is within the physiological range of LDL in human blood/serum. This immunosensor shows high sensitivity of 32.08 μA/mgdl^{-1} cm^{-2} and low detection limit of 0.05 mg/dl. The observed high value of association rate constant (3.24 kM^{-1} s^{-1}) indicates strong affinity of the AAB conjugated CdS QDs towards LDL molecules. This smart immunosensor offers good reproducibility and specificity towards LDL detection. Efforts should be made to utilize this biosensing platform for detection of other biomolecules including cholesterol and high density lipoprotein (HDL).

Acknowledgements

We thank Director, CSIR-National Physical Laboratory, New Delhi, India for the facilities. The financial support received from Department of Science and Technology, India (Grant No. DST/TSG/ME/2008/18) is gratefully acknowledged.

References

1 I. L. Medintz, H. T. Uyed, E. R. Goldman and H. Mattoussi, *Nat. Mater.*, 2005, **4**, 435-446.

2 R. Freeman, J. Girsh, B. Willner and I. Willner, *Isr. J. Chem.*, 2012, **52**, 1125-1136.

3 W. C. W. Chan and S. Nie, Science, 1998, **281**, 2016.

4 X. Gao, Y. Cui, R. M. Levenson, L. W. K. Chung and S. Nie, *Nat. Biotechnol.*, 2004, **22**, 969-976.

5 I. L. Medintz, A. R. Clapp, H. Mattoussi, E. R. Goldman, B. Fisher and J. M. Mauro. *Nat. Mater.*, 2003, **2**, 630-638.

6 B. Dubertret, P. Skourides, D. J. Norris, V. Noireaux, A. H. Brivanlou and A. Libchaber, *Science*, 2002, **298**, 1759-1762.

7 L. Shi, V. D. Paoli, N. Rosenzweig and Z. Rosenzweig. *J. Am. Chem. Soc.*, 2006, **128**, 10378-10379.

8 Y. Xing, Q. Chaudry, C. Shen, K. Y. Kong, H. E. Zhau, L. W. Chung, J. A. Petros, R. M. O'Regan, M. V. Yezhelyev, J. W. Simons, M. D. Wang and S. Nie, *Nat. Protoc.*, 2007, **2**, 1152-1165.

9 X. Michalet, F. F. Pinaud, L. A. Bentolila, J. M. Tsay, S. Doose, J. J. Li, G. Sundaresan, A. M. Wu, S. S. Gambhir and S. Weiss. *Science*, 2005, **307**, 538-544.

10 A. M. Smith, H. Duan, A. M. Mohs and S. Nie. *Adv. Drug Deliv. Rev.*, 2008, **60**, 1226-1240.

11 P. Pericleous, M. Gazouli, A. Lyberopoulou, S. Rizos, N. Nikiteas and E. P. Efstathopoulos *Int. J. Cancer*, 2012, **131**, 519-528.

12 N. Zhu, A. Zhang, P. He and Y. Fang, *Analyst*, 2003, **128**, 260-264.

13 A. Hansen, J. Wang, A.-N. Kawde, Y. X. Kurt, V. Gothelf and G. Collins, *J. Am. Chem. Soc.*, 2006, **128**, 2228-2229.

14 J. A. Ho, Y.-C. Lin, L.-S. Wang, K.-C. Hwang and P.-T. Chou, *Anal. Chem.*, 2009, **81**, 1340-1346.

15 J. Qian, S. Yan, Z. Xiao, *Science*, 2012, **366**, 130–134.

16 Md. A. Ali, S. Srivastava, M. K. Pandey, V. V. Agrawal, R. John and B. D Malhotra, *Anal. Chem.*, 2014, **86**, 1710–1718.

17 Md. A. Ali, P. R. Solanki, M.K. Patel, H. Dhayani, V.V. Agrawal, R. John and B. D. Malhotra, *Nanoscale*, 2013, **5**, 2883-2891.

18 T. Kavitha and H. Yuvaraj. *J. Mater. Chem.*, 2011, **21**, 15686-15691.

19 P. R. Solanki, A. Kaushik, V. V. Agrawal and B. D. Malhotra, *NPG Asia Mater.*, 2011, **3**, 17-24.

20 X. Luo, A. Morrin, A. J. Killard and M. R. Smyth, *Electroanalysis*, 2006, **18**, 319-326.

21 A. Salimi, E. Sharifi, A. Noorbakhsh and S. Soltanian, *Biosens. Bioelectron.*, 2007, **22**, 3146–3153.

22 J. Cao, J.-Z. Sun, H.-Y. Li, J. Hong and M. Wang, *J. Mater. Chem.,* 2004, **14**, 1203-1206.

23 J. Zhu, D. Yang, J. Geng, D. Chen and Z. Jiang, *J. Nanopart. Res.*, 2008, **10**, 729-736.

24 H. Wang, Y. Bai, H. Zhang, Z. Zhang, J. Li and L. Guo. *J. Phys. Chem.* C, 2010, **114**, 16451-16455.

25 Md. A. Ali, K. Kamil Reza, S. Srivastava, V. V. Agrawal, R. John and B. D. Malhotra. *Langmuir,* 2014, **30**, 4192-4201.

26 Md. A. Ali, S. Srivastava, P. R. S. V. Reddy, V. V. Agrawal, C. Kim, R. John and B. D. Malhotra. *Sci. Rep.,* 2013, **3**, 1-9.

27 K. Mondal, Md. A. Ali, V. V. Agrawal, B. D. Malhotra and A. Sharma, *ACS Appl. Mater. Interfaces*, 2014, **6**, 2516-2527.

28 Z. Matharu, S. K. Arya, G. Sumana, V. Gupta and B. D. Malhotra, *J. Mol. Recogn.*, 2008, **21**, 419-424.

29 G. Jie, B. Liu, H. Pan, J. Zhu and H. Chen, *Anal. Chem.,* 2007, **79**, 5574−5581.

30 W. Yan, X. Chen, X. Li, X. Feng, and J.-J. Zhu, *J. Phys. Chem. B,* 2008, **112**, 1275-1281.

31 H. Chammem, I. Hafaid, N. Bohli, A. Garcia, O. Meilhac, A. Abdelghani, L. Mora, *Talanta*, 2015, **144**, 466–473.

32 G. C.-Miranda, E. H. G. Y.-Kanashiro, M. Gidlund and M. G. F. Sales, *J. Mater. Chem. B*, 2014, **2**, 477.

33 Md. A. Ali, N. Singh, S. Srivastava, V. V. Agrawal, R. John, M. Onoda, B. D. Malhotra, *Appl. Biochem. Biotechnol*., 2014, 174, 926–935.

34 H. Dhyani, Md. A. Ali, M. K. Pandey, B. D. Malhotra and P. Sen. *J. Mater. Chem.*, 2012, **22**, 4970-4976.

35 K. M. Okuno, K. Kerman, Y. Takamura, K. Matsumoto and E. Tamiya, *Biosens. Bioelectron.,* 2007, **22**, 2377–2381.

36 Z. Matharu, G. Sumana, M. K. Pandey, V. Gupta and B. D. Malhotra, *Thin Solid Films*, 2009, **518**, 719-723.

37 Z. Matharu, A. J. Bandodkar, G. Sumana, P. R. Solanki, E. M. I. M. Ekanayake, K. Kaneto, V. Gupta and B. D. Malhotra, *J. Phys. Chem. B*, 2009, **113**, 14405-14412.

Figure legends

Figure 1(i) XRD studies of (a) NiO/ITO film and (b) CysCdS-NiO/ITO film, (ii) FT-IR spectra of the various fabricated electrodes and (iii) UV-visible studies of CysCdS QDs (a), NiO/ITO (b) and CysCdS-NiO/ITO film (c).

Figure 2 TEM image of (a) NiO nanorods bundle (inset: individual highly crystalline NiO nanorod), (b) overview of L-cysteine capped CdS QDs (inset: zoom image of CysCdS QDs), (c) after CysCdS incorporation with NiO nanorods and (d) lattice fringes of CysCdS-NiO and (e) selected area electron diffraction pattern of CysCdS-NiO.

Figure 3(i) Cyclic voltammetry (CV) studies of various fabricated electrodes, (ii) CV studies of BSA-AAB/CdS-NiO/ITO immunoelectrode as a function of scan rate [20-100 mV/s] and (iii) electrochemical impedance spectroscopy (EIS) studies of the various fabricated electrodes.

Figure 4(i) Response studies of the immunoelectrode (BSA-AAB/CysCdS) using cyclic voltammetry as a function of LDL concentration [5-120 mg/dl] and (ii) electrochemical current vs LDL concentration plot. (iii) Response studies of the immunoelectrode (BSA-AAB/CdS-NiO) using CV as a function of LDL concentration, (iv) electrochemical current versus LDL concentration plot and (v) current vs. LDL concentrations for both immunosensors. (vi) Response studies of the immunoelectrode (BSA-AAB/CdS-NiO) using CV as a function of LDL real sample from human serum, inset: histogram for magnitude of current response for both real and standard samples.

Schematic 1 shows the fabrication steps relating to fabrication of the immunosensor (BSA-AAB/CdS-NiO) for LDL detection.

Figures

Figure 1

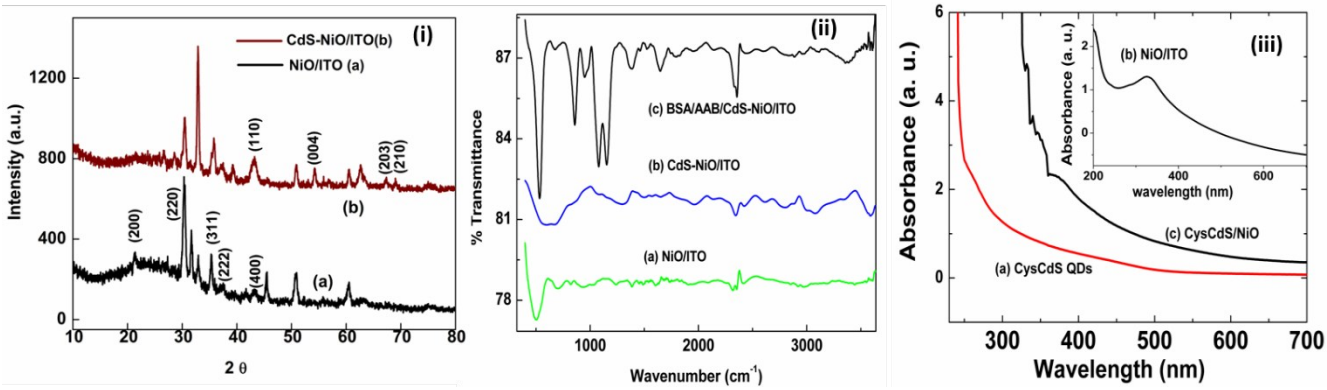

Figure 2

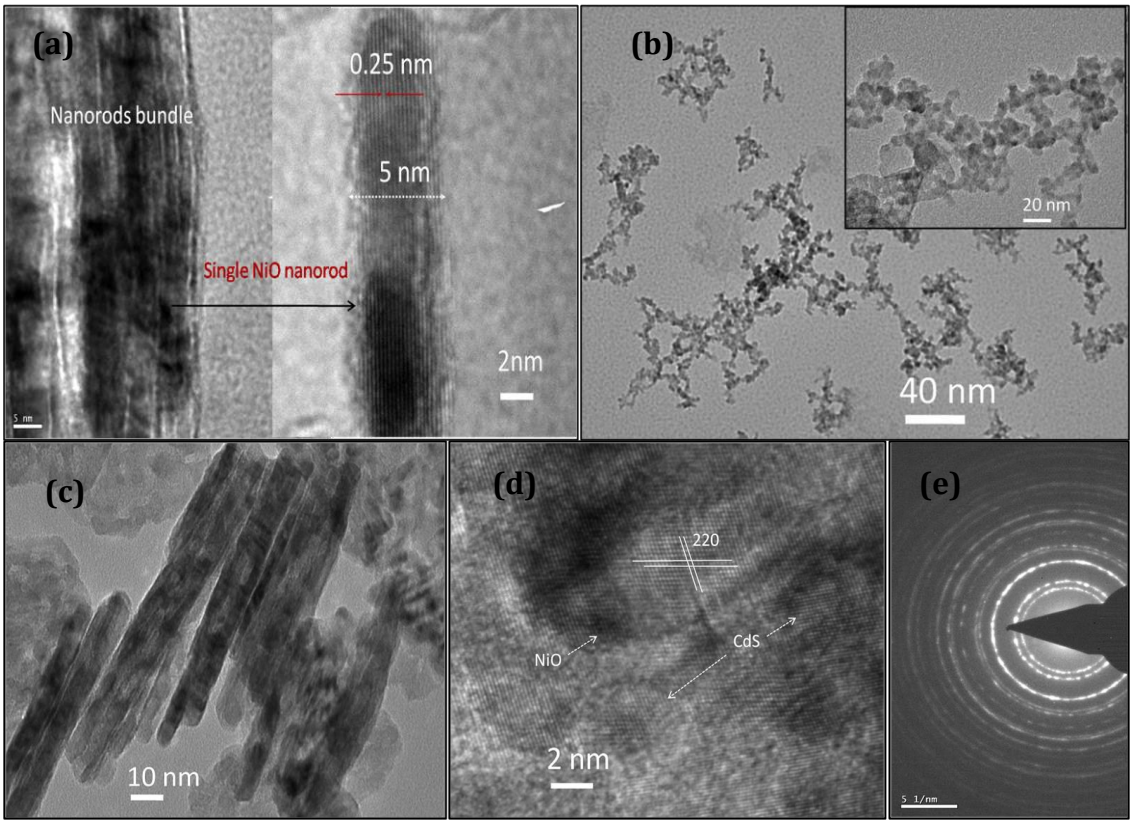

Figure 3

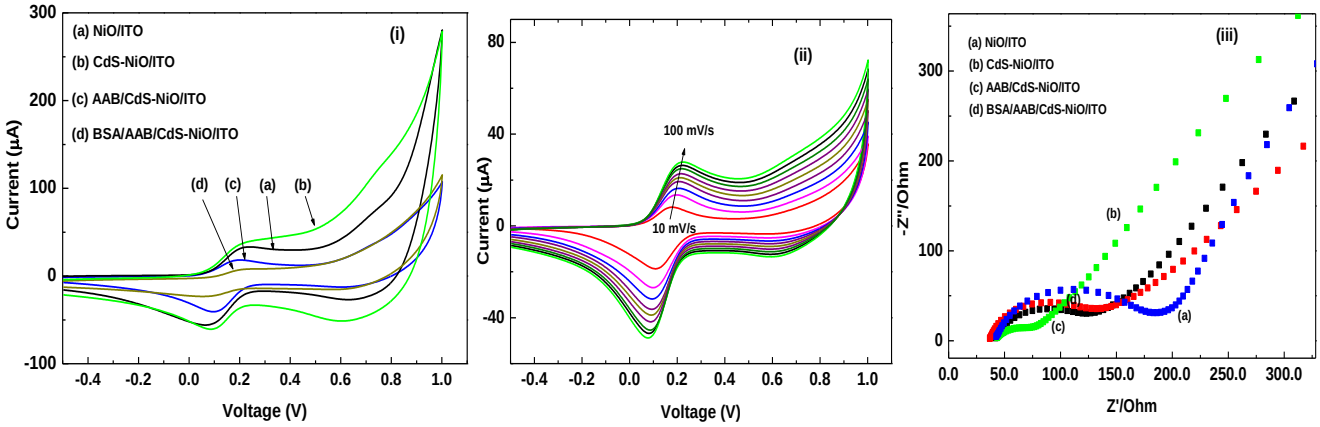

Figure 4

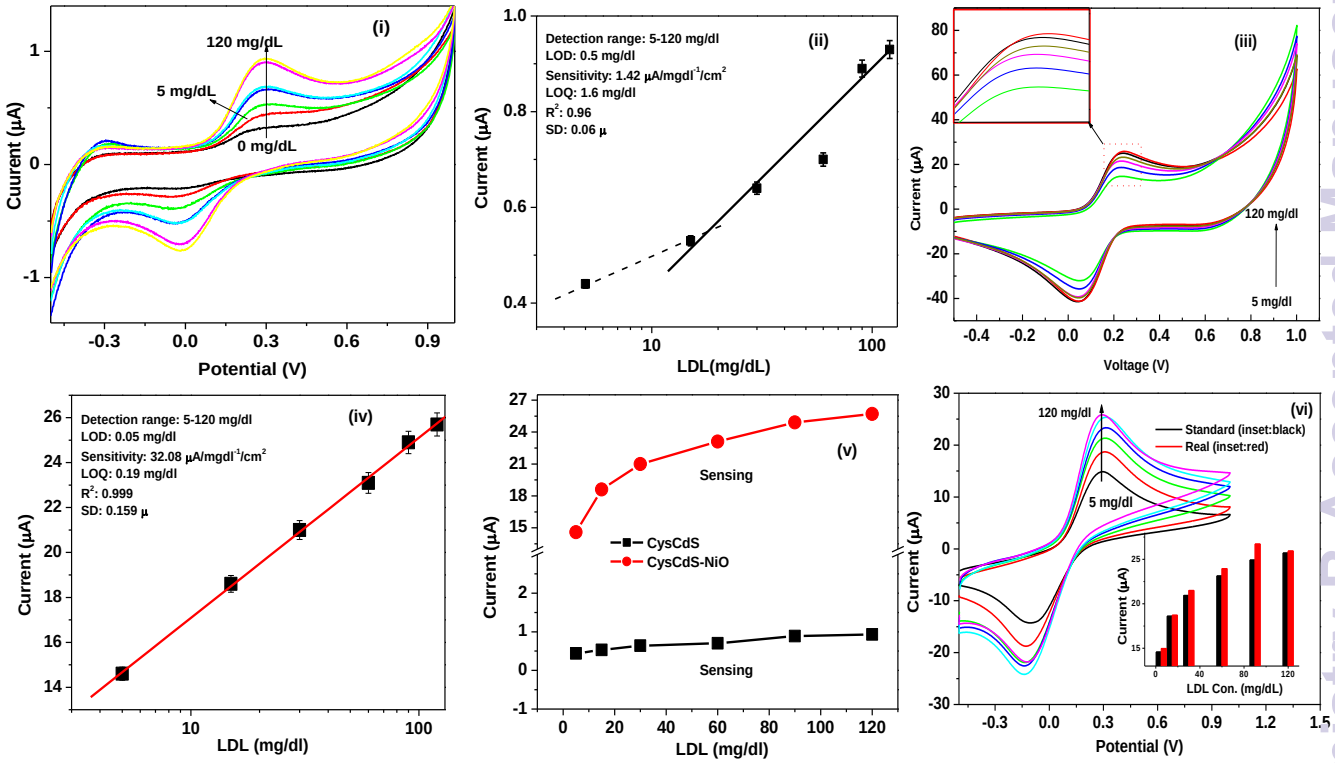

Schematic 1

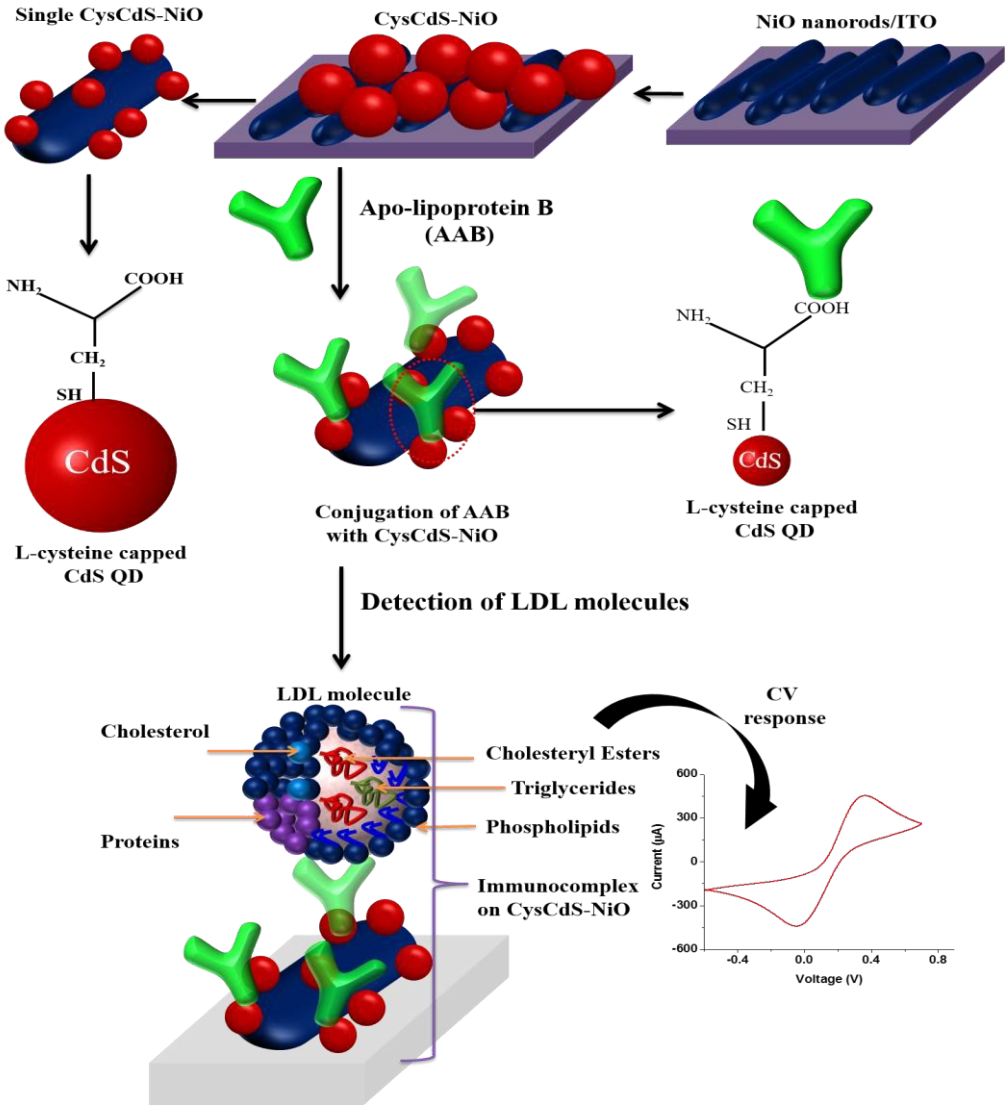

Graphical Abstract

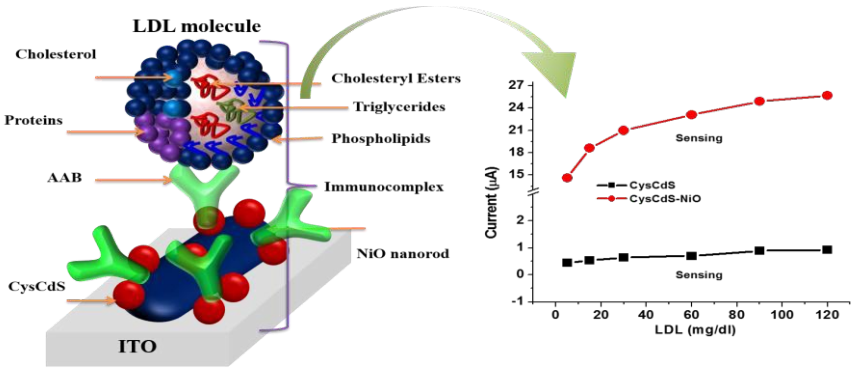

A label-free and sensitive immunosensor has been fabricated using antibody conjugated CdS-NiO nanocomposite for detection of lipid in serum samples.